ACS Catalysis

Research Article

pubs.acs.org/acscatalysis

Hydrothermally Stable, Conformal, Sulfated Zirconia Monolayer Catalysts for Glucose Conversion to 5-HMF

Amin Osatiashtiani,[†] Adam F. Lee,[†] Marta Granollers,[‡] D. Robert Brown,[‡] Luca Olivi,[∥] Gabriel Morales,[§] Juan A. Melero,[§] and Karen Wilson*[,†]

[†]European Bioenergy Research Institute (EBRI), Aston University, Aston Triangle, Birmingham B4 7ET, United Kingdom

[‡]Department of Chemical Sciences, University of Huddersfield, Huddersfield HD1 3DH, United Kingdom

[§]Department of Chemical and Energy Tech, Chemical and Environmental Tech, Mechanical Tech and Analytical Chemistry, Universidad Rey Juan Carlos, C/Tulipan. s/n, E-28933 Móstoles, Madrid, Spain

[∥]Sincrotrone Trieste, AREA Science Park, 34149 Basovizza, Trieste, Italy

Supporting Information

ABSTRACT: The grafting and sulfation of zirconia conformal monolayers on SBA-15 to create mesoporous catalysts of tunable solid acid/base character is reported. Conformal zirconia and sulfated zirconia (SZ) materials exhibit both Brönsted and Lewis acidity, with the Brönsted/Lewis acid ratio increasing with film thickness and sulfate content. Grafted zirconia films also exhibit amphoteric character, whose Brönsted/Lewis acid site ratio increases with sulfate loading at the expense of base sites. Bilayer ZrO_2/SBA-15 affords an ordered mesoporous material with a high acid site loading upon sulfation and excellent hydrothermal stability. Catalytic performance of SZ/SBA-15 was explored in the aqueous phase conversion of glucose to 5-HMF, delivering a 3-fold enhancement in 5-HMF productivity over nonporous SZ counterparts. The coexistence of accessible solid basic/Lewis acid and Brönsted acid sites in grafted SZ/SBA-15 promotes the respective isomerization of glucose to fructose and dehydration of reactively formed fructose to the desired 5-HMF platform chemical.

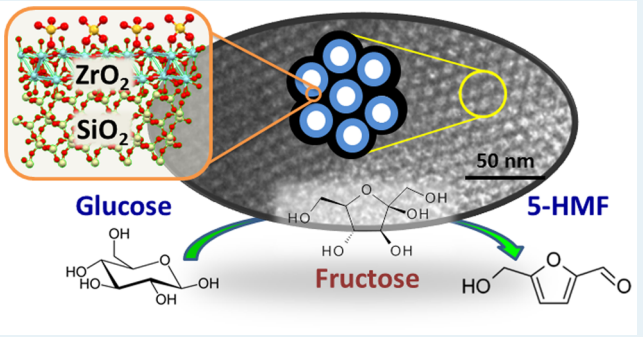

KEYWORDS: *SBA-15, sulfated zirconia, solid acid, 5-HMF, hydrothermal stability, solid base*

1. INTRODUCTION

The quest for sustainable resources to meet the demands of a rapidly rising global population while reducing anthropogenic CO_2 emissions and associated climate change represents one of this century's grand challenges. If average global temperature rises induced by greenhouse gases are not to exceed 2 °C, then estimates indicate that a large proportion of oil, gas, and coal reserves must remain untouched.[1] Biomass offers the most readily implemented and low cost solution for carbon-neutral transportation fuels[2] and the only nonpetroleum route to organic molecules for the manufacture of bulk, fine, and specialty chemicals[3] and polymers[4] required to meet future societal demands. Akin to petroleum refining, biorefining will integrate biomass conversion processes to produce fuels, power, and chemicals, thereby increasing the economic viability of bioderived processes.[5] In this respect, lignocellulosic biomass offers great potential for green production of fuels and chemicals.[6] Among these chemicals, 5-hydroxymethylfurfural (5-HMF),[7] identified by the U.S. DOE[8,9] as a versatile intermediate for the production of value-added chemicals and high performance liquid fuels, has attracted worldwide attention.[10]

Aqueous phase, hydrothermal processing of cellulose and sugars offers an attractive method to produce platform chemicals and fuels.[11] In a biorefinery, aqueous sugar streams may be produced from lignocellulose via fractionation methods such as steam explosion and enzymatic hydrolysis.[12] The development of heterogeneous catalysts for aqueous phase conversion of such resources requires materials with improved hydrothermal stability.[13] Furthermore, it would be desirable for catalysts to exhibit bifunctional properties, such as tunable acid/base character to initiate cascade reactions in biomass conversion processes.[14] Carbon, zirconia, and titania supports[15] are among materials reported to exhibit excellent hydrothermal stability and desirable characteristics for applications in biomass processing. However, in their native form, they exhibit low surface areas and offer limited control over internal porosity, which restricts their application for the chemical conversion of bulky biobased molecules.

Received: May 8, 2015
Revised: June 1, 2015
Published: June 2, 2015

DOI: 10.1021/acscatal.5b00965
ACS Catal. 2015, 5, 4345−4352

We reported previously on the aqueous phase conversion of glucose to 5-HMF using a bifunctional sulfated zirconia (SZ) catalyst, in which the amphoteric nature of zirconia was exploited in conjunction with controlled surface sulfation to tune the acid−base properties.[16] Tailoring the acid/base distribution can generate a material with the necessary base sites for glucose → fructose isomerization and Brönsted acid sites optimized for the subsequent conversion of reactively formed fructose to 5-HMF. Although such nonporous zirconias are promising, their intrinsic rate of 5-HMF productivity requires significant enhancement to improve catalyst efficiency and underpin a commercial process. Methods to stabilize highly porous or dispersed tunable ZrO_2 and SO_4/ZrO_2 phases are thus required.[17]

The direct synthesis of mesoporous ZrO_2 and ZrO_2/SiO_2 has been reported via sol−gel[18−21] or coprecipitation methods;[22,23] however, poor thermal stability and associated pore-collapse during catalyst activation has limited the utility of such templated zirconias.[24,25] Robust high-surface-area supports such as nanostructured silicas (e.g., HMS-24,[26] MCM-41, and SBA-15) have the potential to serve as high-area scaffolds with well-defined mesoporosity over which to disperse ZrO_2, but to maintain the internal pore network and, hence, molecular accessibility, it is critical that zirconia be introduced in a layer-by-layer fashion so as to minimize the formation of low area three-dimensional crystallites and pore blockage. Incipient wetness impregnation,[27−32] urea hydrolysis,[33] and vapor-induced hydrolysis (VIH)[25,34] methods have been reported to prepare ZrO_2 coatings on SBA-15, typically employing zirconium propoxide[27−31] or acetate[11] precursors in an anhydrous organic solvent (e.g., dry hexane or 50:50 vol % anhydrous toluene/ethanol). However, simple variation of the precursor concentration to achieve different zirconia loadings invariably yields 3−4 nm crystallites, similar to the silica mesopore diameter. VIH methods employing zirconium oxychloride ($ZrOCl_2{\cdot}8H_2O$) or zirconyl nitrate[25] precipitation with urea or NH_3/water have succeeded in introducing zirconium hydroxide within SBA-15 mesopores; however, attempts to sulfate the resulting zirconia films yield a material prone to S leaching.[34]

Here, we report a synthetic route to high-area SZ/SBA-15 catalysts possessing good textural properties and molecular access to in-pore ZrO_2 and SO_4 active sites. The evolution of acid/base properties was explored as a function of the thickness and degree of sulfation of conformal zirconia monolayers (MLs), and the resulting physicochemical properties correlated with catalytic performance in the aqueous phase telescopic conversion of glucose → fructose → 5-HMF.

2. EXPERIMENTAL SECTION

2.1. Catalyst Preparation. ZrO_2-grafted SBA-15 was synthesized according to our previous report.[35] Briefly, 10 g of SBA-15 (prepared via the original method of Zhao et al.[36]) was dried at 300 °C for 4 h, then cooled to 100 °C and added to a solution of 58.5 g of 70% zirconium propoxide in propanol (Sigma-Aldrich) in 300 mL of anhydrous hexane. The amount of zirconium precursor was calculated on the basis of the number of surface hydroxyl groups on SBA-15 (determined from thermal gravimetric analysis). By working in dry solvent, it was hoped that the reaction would be confined between the surface hydroxyls and zirconium propoxide, favoring conformal monolayer growth over the SBA-15 surface. The reaction mixture was refluxed at 69 °C overnight, filtered, and washed three times with hexane to remove any unreacted precursor. The material was subsequently rehydrated in 300 mL of deionized water under stirring for 4 h to fully hydrolyze any residual propoxide groups. Finally, the catalyst was filtered and dried at 80 °C overnight. This procedure was repeated to produce SBA-15 coated with a nominal second and third monolayer of zirconia. Sulfation of ZrO_2/SBA-15 materials was achieved via their immersion in aqueous sulfuric acid (10 mL acid solution per g sample, H_2SO_4 concentrations spanning 0.005−0.25 M) for 5 h, after which samples were filtered and dried overnight at 80 °C. The resulting materials were activated by calcination at 550 °C in static air for 3 h.

2.2. Catalyst Characterization. N_2 porosimetry was performed on either a Micromeritics Tristar 3000 or Quantachrome Nova 4000 porosimeter, with BET surface areas calculated over the range P/P_0 = 0.03−0.19, wherein a linear relationship was maintained. Pore size distributions were obtained by applying the BJH model to the desorption branch of the isotherm. Structural order was evaluated by means of low-angle X-ray powder diffraction (XRD) on a Bruker D8 Advance diffractometer using the Cu Kα line in the range 2θ = 0.6−5.0° with a step size of 0.02°, with phase identification evaluated by wide angle XRD in the range 2θ = 10−80° with a step size of 0.04°. HRTEM measurements were performed on a Philips TECNAI-20T electronic microscope operated at 200 kV. Bulk zirconium contents were determined by scanning electron microscopy (SEM) on a Philips XL 30 ESEM electronic microscope equipped with EDX. X-ray photoelectron spectroscopy (XPS) was performed on a Kratos Axis HSi photoelectron spectrometer equipped with a charge neutralizer and Mg Kα X-ray source ($h\nu$ = 1253.6 eV). Spectra were recorded at normal emission with an analyzer pass energy of 20 eV and X-ray power of 225 W. ZrO_2 film thicknesses were calculated from the attenuation of the Si 2p signal using eq 1,

$$I = I_0 \exp\left(\frac{-\alpha}{\lambda \cos\theta}\right) \tag{1}$$

where I is the peak intensity, I_0 is the intensity of the clean SBA-15 surface, λ is the inelastic mean free path for Si 2p photoelectrons taken to be 1.26 nm, d is the film thickness, and θ is the angle of photoelectron emission.[37,38]

Acid and base site loadings and adsorption enthalpies were determined via adsorption flow calorimetry of NH_3 and SO_2, respectively, on a Setaram DSC111 system connected to gas flow and switching systems. Samples were outgassed at 450 °C under flowing N_2 (10 mL min^{-1}) for 2 h prior to pulse titration at 150 °C. A steady 10 mL min^{-1} flow of N_2 was maintained across the sample for 3 h at 150 °C to effect activation. A sequence of 10 probe gas pulses (1 vol % of probe gas in N_2) were delivered to the carrier gas stream from a 2 mL sample loop for NH_3/SO_2 using a two-position Valco valve with an automated microelectric actuator. Heat output associated with interaction between the probe gas and the sample was detected by DSC, and the concentration of NH_3/SO_2 in the gas flow downstream of the DSC was measured with a HPR 20 Hiden MS gas analyzer via a heated capillary at 175 °C. The time between pulses was 90 min for NH_3 and 30 min for SO_2 to allow desorption of any reversibly adsorbed probe gas back into the pure N_2 stream, or redistribution onto the sample, and baseline stabilization. Temperature-programmed desorption was performed on probe-saturated samples by ramping the temperature from 150 to 400 °C at 5 °C min^{-1}.

DOI: 10.1021/acscatal.5b00965
ACS Catal. 2015, 5, 4345−4352

Ex situ pyridine adsorption was performed by exposure of diluted samples (10 wt % in KBr) to pyridine vapor overnight. Excess physisorbed pyridine was removed in vacuo at 30 °C prior to recording in vacuo diffuse reflectance infrared Fourier transform (DRIFT) spectra at 50 °C in an environmental cell. Spectra were obtained using a Nicolet Avatar 370 MCT with Smart Collector accessory. Zr K-edge transmission X-ray absorption spectroscopy (XAS) was performed at the XAFS beamline of the Elettra synchrotron with a Si(111) double-crystal monochromator at 250 mA/2 GeV.

2.3. Catalytic Tests. Kinetic studies of glucose (Sigma-Aldrich 99.5%) and fructose (Sigma-Aldrich 99%) conversion were conducted in a Radleys Starfish carousel reactor under stirred batch conditions at 100 °C. Reactions were performed using 0.1 g of reactant, 0.1 g of catalyst, and 20 mL of deionized water. Samples were withdrawn periodically and filtered prior to analysis on an Agilent 1200 series HPLC equipped with refractive index and UV diode array detectors, and a Hi-Plex H column. Product yields and selectivity were calculated on a carbon basis according to eqs 2 and 3.

$$\text{yield}\ (\%) = \frac{(\text{moles of C in product})}{(\text{moles of C in reactant at } t = 0)} \times 100 \quad (2)$$

$$\text{selectivity}\ (\%) = \text{yield} \times \frac{100}{(\text{reactant conversion})} \quad (3)$$

Mass balances were determined based on the moles of carbon in the identified products, relative to those in the reactant according to eq 4:

$$\frac{C_{out}}{C_{in}}\ (\%) = \sum \frac{(\text{moles of C in product + remaining reactant})}{(\text{moles of C in reactant at } t = 0)} \times 100 \quad (4)$$

Initial reaction rates were determined during the first 3 h when conversion profiles were linear and <25%, with resulting activities reported normalized per mass of either catalyst or zirconium. It should be noted that low reaction temperatures were selected for this study to minimize background rates for glucose and fructose conversion and to facilitate the detailed study of catalyst acid−base properties on activity.

2.4. Hydrothermal Stability. The hydrothermal stability of SBA-15 and ZrO_2/SBA-15 was evaluated in a Parr 5513 autoclave. The reactor was charged with 30 mL of deionized water and 0.1 g of catalyst, sealed and heated to 170 °C under vigorous stirring for 6 h. Materials were held at this temperature at ∼7 bar autogenous pressure, then cooled to room temperature, recovered by filtration, and then dried at 80 °C overnight prior to analysis of textural properties by porosimetry and XRD.

3. RESULTS AND DISCUSSION

3.1. ZrO_2 and SZ Film Growth. The successful stepwise growth of zirconia monolayers over SBA-15 was first verified by a combination of porosimetry, HRTEM, XRD, and XPS. Nitrogen porosimetry revealed that all materials exhibited type IV isotherms and steep H1 hysteresis loops typical of mesostructured SBA-15 with a narrow mesopore size distribution (Figures S3, S4).[39] The composition and textural properties of the parent SBA-15 and ZrO_2 grafted samples are reported in Tables S1, S2 as a function of nominal monolayers of ZrO_2 and are in accordance with our recent communication.[22] Pore volume, mean mesopore diameter, and BET surface area decreased progressively with each grafting cycle, which is consistent with a layer-by-layer growth mode of zirconia throughout the mesopore network, resulting in thickening of the mesopore walls and a concomitant reduction of the mesopore diameter. Low-angle XRD (Figure S1) also confirmed that the mesostructured order of SBA-15 was retained, with materials exhibiting a main peak at 2θ = ∼1° and two weaker features at 2θ = 1.7° and 1.9° attributed to the (100), (110) and (200) reflections, respectively, of the *pmm6* hexagonally ordered parent support.[36,40]

The highly dispersed nature of the incorporated ZrO_2 was verified by the absence of monoclinic or tetragonal phase diffraction features in the wide-angle XRD region, indicating dimensions below the instrumental detection limit of ∼2 nm. These observations are supported by HRTEM, which visualized an ordered hexagonal SBA-15 mesophase with uniform pore walls following Zr grafting, with no evidence for crystalline zirconia deposits, even after three grafting cycles (Figure 1a).

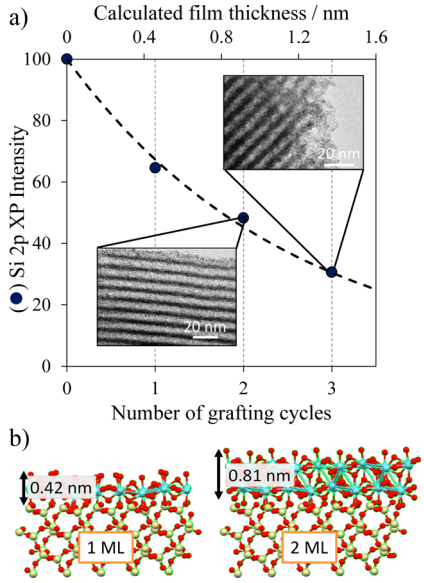

Figure 1. (a) Attenuation of Si 2p XP signal of ZrO_2/SBA-15 as a function of zirconia grafting cycle (dashed line shows the theoretical attenuation predicted from eq 1). Inset shows HRTEM of pore channels following 2 and 3 grafting cycles. (b) Estimated film thickness for 1 and 2 ML ZrO_2 over a SiO_2 substrate.

Layer-by-layer growth of zirconia overlayers was verified by XPS via attenuation of the Si 2p signal; Figure 1a reveals an exponential decay in the SBA-15 substrate intensity with consecutive zirconia depositions. The first and second grafting cycles attenuated the substrate by 35.6 and 51.9%, equating to 0.5- and 0.84-nm-thick overlayers of ZrO_2, respectively, in excellent agreement with the estimated thicknesses of (111)-oriented mono- and bilayers of ZrO_2 (Figure 1b), confirming their conformal nature.

Sulfation of the 1−3 ML ZrO_2/SBA-15 samples was subsequently performed by impregnation with 0.075 M H_2SO_4 (the concentration previously reported to afford optimum acid site properties)[16] and calcination at 550 °C. The absence of any new XRD feastures postsulfation confirmed the absence of large SZ crystallites. Furthermore, the Zr/Si atomic ratios from XPS and EDX were unchanged by sulfation, suggesting no change in the film morphology from the parent zirconia overlayer (e.g., sulfate-induced sintering).

DOI: 10.1021/acscatal.5b00965
ACS Catal. 2015, 5, 4345−4352

The bulk and surface S/Zr atomic ratios fell with initial ZrO_2 thickness, indicating only the terminating zirconia layer underwent sulfation (Table S2).

The acid site strength, loading, and nature was probed by a combination of NH_3 calorimetry and pyridine titration. Figure 2 shows NH_3 pulse calorimetry profiles for SZ/SBA-15, which

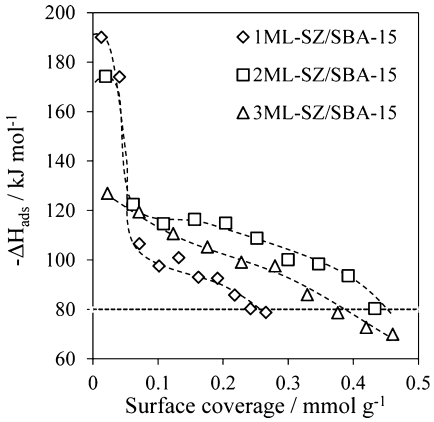

Figure 2. NH_3 pulse calorimetry of 1−3 ML of SZ/SBA-15.

evidence predominantly moderate strength acidic sites ($-\Delta H_{ads}$ ~ 100−120 kJ mol^{-1}), which is comparable to those in bulk SZ catalysts.[16] The 1 and 2 ML SZ/SBA-15 samples also exhibit a small proportion of strong acid sites with $-\Delta H_{ads}$ ~ 180−200 kJ mol^{-1}. Although the precise origin of these strong acid sites is unclear, they likely originate through the truncated nature of the ZrO_2 monolayers and corresponding defective (uncoordinated Zr^{4+}) centers, which may confer strong Lewis acidity, being electronically perturbed by the underlying silica.[41] This hypothesis is supported by pyridine titration and quantification of the resultant DRIFT spectra[42] (Figures 3 and S7) which

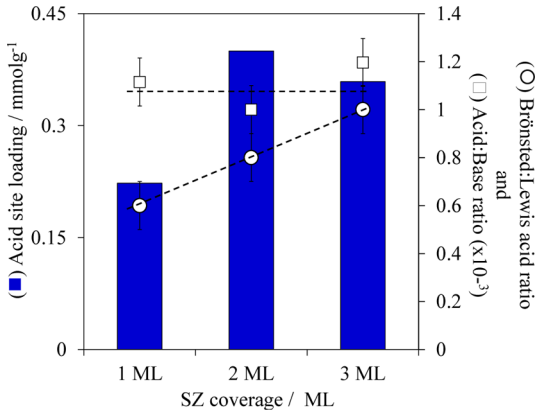

Figure 3. Acid and base properties of 1−3 ML of SZ/SBA-15.

show a switchover from Lewis to Brönsted acidity with increasing ZrO_2 film thickness. The Zr 3d XP spectra (Figure S5) also exhibits a shift to a lower binding energy with increased layer thickness, demonstrating the electron-deficient nature of the first layer at the SiO_2 interface. The maximum acid site density (Figure 3) was following sulfation of a zirconia bilayer. Interfacial zirconia thus appears more chemically inert due to either perturbation by the underlying SBA-15 support or an inability to crystallize in the requisite tetragonal phase known to impart superacidity.[43] The acid/base density was independent of zirconia film thickness, being dominated by solid acid character.

The highly dispersed nature of the conformal ZrO_2 monolayers prohibited their phase analysis by conventional powder XRD; hence, Zr K-edge XAS was performed to inform the structure of both zirconia and SZ films. The common cubic, tetragonal, and monoclinic ZrO_2 phases exhibit characteristic XANES spectra whose line shape and width are dictated by symmetry-dependent splitting of the 1s → 4d transition.[44,45] Symmetrical cubic ZrO_2 (8-coordinate Zr^{4+}) affords a sharp edge jump and two well resolved transitions to e_g and t_{2g} valence states. In contrast, tetragonal (8-coordinate Zr^{4+}) and monoclinic (7-coordinate Zr^{4+}) phases possess lower symmetry, leading to further splitting of the Zr 4d valence band.

Tetragonal ZrO_2 K-edge XANES split into four (a_1, b_1, e, and b_2) bands that are typically resolved as a doublet, whereas the monoclinic phase possesses five nonresolvable states observed as a featureless single peak at the white line. Figure 4 shows that

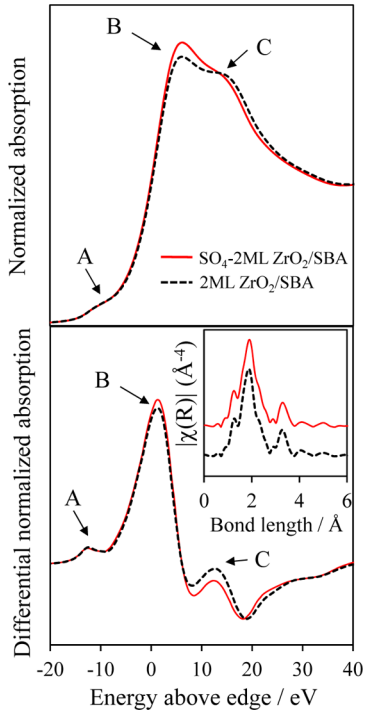

Figure 4. Normalized and derivative Zr K-edge XANES of 2 ML ZrO_2/SBA-15 and 2 ML SZ/SBA-15. Inset shows corresponding radial distribution functions from the EXAFS spectra.

the 2 ML ZrO_2/SBA-15 exhibits three distinct features: a weak pre-edge feature labeled A, and a split white line labeled B and C, which are more clearly discerned in the derivative spectra.

Tetragonal ZrO_2 comprises two nonequivalent tetrahedral ZrO_4 units, with different Zr−O bond lengths. Enhanced s−p mixing in tetrahedral geometries[45,46] gives rise to an extra electronic state, ~6−7 eV, below the Zr K-edge white line that is unique to tetragonal zirconia and consistent with peak A, evidencing the presence of tetragonal ZrO_2 in both ZrO_2/SBA-15 and SZ/SBA-15 materials. Sulfation causes the white line to sharpen, with the lower-energy feature B strengthening at the expense of C, indicating a change in electronic structure. The rise in B is consistent with the changes in symmetry and charge distribution of the Zr local environment expected to accompany their covalent binding to SO_4 groups. The Figure

DOI: 10.1021/acscatal.5b00965
ACS Catal. 2015, 5, 4345−4352

4 inset shows the radial distribution functions of ZrO_2 and SZ films, revealing features at 2.0 and 3.3 Å, attributable to Zr−O and Zr−Zr first coordination shells; the weak Zr−Zr shell consistent with the ultrathin nature of the conformal film that, hence, lacks the complete nearest neighbor shell present within three-dimensional zirconia crystallites.

3.2. Catalytic Activity. The catalytic performance of 1−3 ML SZ/SBA-15 in glucose dehydration to 5-HMF at 100 °C is summarized in Figure 5. Activity for glucose conversion and

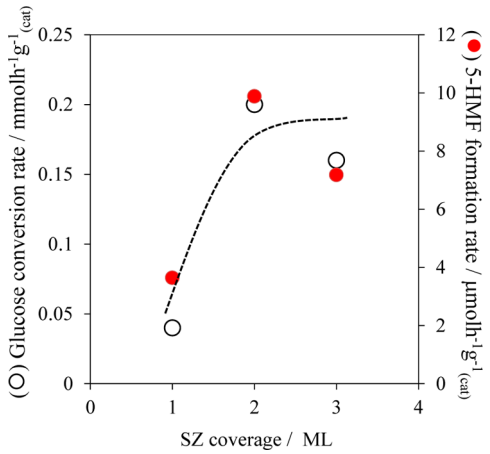

Figure 5. Comparison of activity for glucose conversion and HMF production at as a function of SZ film thickness.

resultant 5-HMF production increases from 1 → 2 ML, showing little further change for 3 ML. Glucose conversion to 5-HMF is proposed to proceed via a Lewis acid (or base)-catalyzed isomerization to fructose, followed by a Brönsted acid-catalyzed dehydration, as shown in Scheme 1. The catalytic

Scheme 1. Glucose Isomerization to Fructose and Subsequent Dehydration to 5-HMF

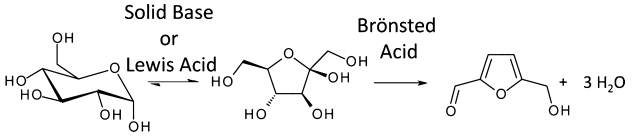

performance mirrors both the total acid site loading and Brönsted/Lewis acid ratio, suggesting that 5-HMF production is rate-limited by the Brönsted acid catalyzed dehydration. This postulate is supported by the observed accumulation of fructose during reaction (Figure S20), which reflects its slower removal through dehydration relative to production via more rapid glucose isomerization.

3.3. Effect of Sulfate Coverage. Our previous studies of bulk SZ demonstrated that the telescopic glucose → fructose → 5-HMF reaction could be tuned through controlling the degree of surface sulfation of the underlying amphoteric zirconia, that is, SO_4 coverage (θ).[16] We hence investigated the impact of θ_{SO_4} on the behavior of the optimal 2 ML ZrO_2/SBA-15 material via impregnation with 0.005−0.25 M H_2SO_4. Low-angle XRD and N_2 porosimetry confirmed retention of the parent SBA-15 structure for all acid molarities (Figures S9, S11), although samples treated with >0.1 M H_2SO_4 induced a slight expansion in the mean mesopore diameter that may indicate a small degree of zirconia redispersion (Table 1). XPS and EDX (Figures S13, S14; Tables S5, S6) confirmed that the Zr content was constant with rising S loading for $[H_2SO_4] \leq 0.05$ M; however, for $[H_2SO_4] \geq 0.1$ M, both S and Zr loadings decreased, suggesting corrosion or dissolution of the ZrO_2 film. This hypothesis was confirmed by the Zr/Si and S/Si surface atomic ratios, both of which fell under aggressive sulfation treatment. SZ films prepared with $[H_2SO_4] < 0.1$ M, with S/Zr < 0.18 therefore appear chemically stable. NH_3 and SO_2 pulse calorimetry mapped the evolution of acid and base site loadings with a S/Zr atomic ratio for the 2 ML SZ/SBA-15 (Figures S15, S16; Table S7); acid sites increased steadily with S content at the expense of base sites, in excellent agreement with previous trends observed for bulk SZ.[16] At S/Zr ratios >0.18, the acid site loading reached a plateau, indicating surface saturation with sulfate species. The mean $-\Delta H_{ads}(NH_3)$ of 110 kJ mol^{-1} was independent of sulfate coverage, indicating a common, predominantly medium strength acid site, consistent with bulk SZ,[16] whereas the mean $-\Delta H_{ads}(SO_2)$ of 100 kJ mol^{-1} for 2 ML ZrO_2/SBA-15 was consistent with values for bulk ZrO_2 that possesses weak/medium base sites; typical heats of adsorption for SO_2 span 60 (for SiO_2) to 215 kJ mol^{-1} (MgO); hence, values for 2 ML SZ/SBA-15 materials of 80−129 kJ mol^{-1} evince mild basicity.[47] The evolution of Brönsted/Lewis acid character with θ_{SO_4} was quantified by pyridine titration and confirmed the expected increase in Brönsted acid character with sulfation (Figure S18).

3.4. Catalytic Activity. The performance of *x*M-SZ/SBA-15 catalysts was subsequently evaluated for 5-HMF production from fructose or glucose. 5-HMF productivity per Zr atom from fructose was directly proportional to the concentration of sulfating solution (i.e., θ_{SO_4}) (Figure S21), whereas in contrast, that from glucose exhibited a maximum for $[H_2SO_4] = 0.02$ M, equivalent to an acid/base atomic ratio of ∼4. These observations are qualitatively consistent with our recent study

Table 1. Structure, Composition and Acid/Base Properties of 2 ML SZ/SBA-15 As a Function of H_2SO_4 Molarity

sample	at. S/Zr (XPS)	surf. area; $m^2\ g^{-1}$	mesopore diam; nm	bulk Zr (EDX); wt %	bulk S (EDX); wt %	acid site loading; mmol g^{-1}	base site loading; mmol g^{-1}
SBA-15		850	6.8	0	0		
2 ML ZrO_2/SBA-15		540	5.4	18.7	0.0	0.233	0.079
0.005 M SZ/SBA-15	0.01	550	5.6	20.7	0.0		
0.01 M SZ/SBA-15	0.02	538	5.6	19.9	0.0	0.275	0.067
0.025 M SZ/SBA-15	0.06	506	5.3	20.0	0.6	0.302	0.039
0.05 M SZ/SBA-15	0.13	547	5.3	18.8	1.3	0.340	0.017
0.1 M SZ/SBA-15	0.18	542	4.3	16.5	1.5	0.397	0.008
0.17 M SZ/SBA-15	0.22	557	5.9	11.8	1.5		
0.25 M SZ/SBA-15	0.42	483	6.3	9.5	1.7	0.347	0.002

DOI: 10.1021/acscatal.5b00965
ACS Catal. 2015, 5, 4345−4352

of fructose conversion over bulk SZ catalysts and in quantitative agreement with that for glucose conversion wherein maximal 5-HMF productivity was attained for a bulk SZ surface with an identical mix of acid/base character. The rise in 5-HMF production from fructose with surface sulfation can be simply understood in terms of the concomitant increase in the Brönsted acidity and, hence, dehydration activity, whereas glucose conversion to 5-HMF requires a balance of surface base/Lewis acid sites (to drive isomerization to fructose) and Brönsted acid sites (for the subsequent dehydration). Despite similarities in the catalytic behavior of *x*M-SZ/SBA-15 and bulk SZ materials, the high-area conformal SZ monolayers delivered a far superior performance with respect to 5-HMF productivity per Zr atom: three (two) times more active for glucose (fructose) conversion than bulk SZ analogues (Figure 6).

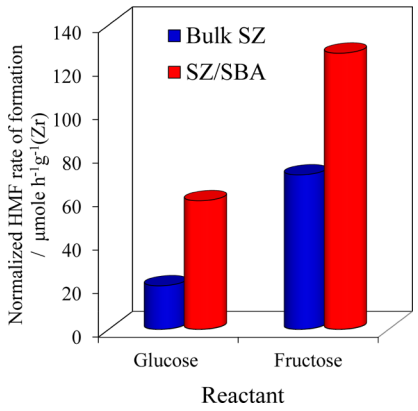

Figure 6. Zr-normalized 5-HMF productivity from glucose and fructose over the optimum bulk SZ and SZ/SBA-15 catalysts. (SZ and SZ/SBA prepared from impregnation with 0.02 M H_2SO_4 or 0.1 M H_2SO_4 for glucose or fructose reactions, respectively).

This difference may reflect the greater dispersion of the thin film system and increased Lewis character of the grafted SZ film compared to bulk SZ and, hence, improved glucose isomerization of the former. In this respect, we note that although Lewis acids are claimed to be more selective than strong bases such as $Ca(OH)_2$ or $Mg(OH)_2$ for glucose → fructose isomerization[48] (which promote undesired degradation via reverse aldol reactions[49]), in this work, the mild basicity of ZrO_2 seems important in promoting 5-HMF formation at low surface θ_{SO_4}.The recyclability of our SZ/SBA-15 materials in glucose conversion to 5-HMF was evaluated for two of the most active catalysts, which were recovered after 6 h reaction, dried, and recalcined. Recycled catalysts retained their activity for glucose dehydration, confirming their robust nature (Figures S22, 23).

3.5. Hydrothermal Stability. Heterogeneous catalysts that possess excellent hydrothermal stability are essential to the development of aqueous phase biomass processing. Although the reaction temperatures used in this work were mild, related biomass processes operate between 140 and 180 °C, a regime wherein ordered mesoporous silicas such as SBA-15 exhibit poor hydrothermal stability,[36,50−52] hindering their wider utility.[53] Because bulk ZrO_2 is considered hydrothermally stable, we speculated that dispersion of zirconia over SBA-15 could improve the support stability in high-temperature water. Figure 7 shows pore size distributions and low-angle XRD patterns for as-synthesized and 2 ML ZrO_2/SBA-15 before and after heating in water at 170 °C for 6 h.

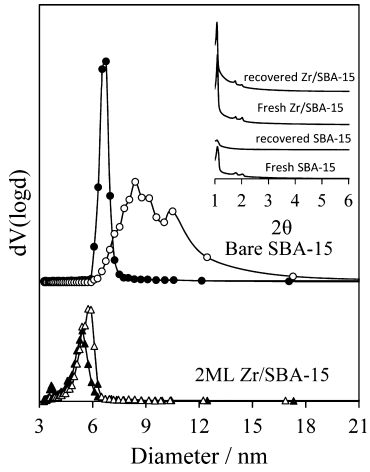

Figure 7. BJH pore size distributions before (solid symbols) and after (open symbols) hydrothermal treatment of parent SBA-15 (●) and 2 ML ZrO_2/SBA-15 (▲). Inset shows low-angle XRD of as-prepared and posthydrothermally treated materials.

The parent SBA-15 underwent pore collapse, evidenced by loss of low-angle diffraction features and simultaneous broadening of the pore distribution. The zirconia-grafted SBA-15, by contrast, retained an ordered pore network with uniform, narrow mesopores. Hence, it can be concluded that grafting zirconia is beneficial to hydrothermal stability of the SBA-15 support. Dissolution of amorphous silica has been reported by many research groups,[54−56] even at room temperature.[57] Although silica dissolution from SBA-15 leads to loss of order and pore expansion, the zirconia film protects the SBA-15 support and the structure of the support remains intact.

4. CONCLUSIONS

A conformal grafting method has been employed to grow ZrO_2 monolayers over a mesoporous SBA-15 framework. XAS, XPS, and DRIFTS analysis confirms that subsequent wet impregnation with H_2SO_4 results in highly dispersed sulfated tetragonal zirconia monolayers whose acid site density and Brönsted/Lewis acid site ratio is optimal for a 2 ML SZ film. The acid/base properties of these conformal SZ films can be readily tuned by varying the concentration of the sulfating solution, with a high $[H_2SO_4]$ favoring Brönsted surface acidity. These 2 ML SZ/SBA-15 catalysts were examined toward the aqueous phase conversion of glucose to 5-HMF, displaying significant greater per site rate enhancements for 5-HMF production than bulk SZ counterparts under identical reaction conditions. Coexisting basic and Lewis acid sites (associated with zirconia exposed within partially sulfated conformal ZrO_2 films) in SZ/SBA-15 materials promote glucose isomerization to fructose, whereas Brönsted acid (sulfate) sites direct fructose dehydration to 5-HMF. Although the absolute performance of our sulfated Zr-SBA-15 catalysts is not exceptional compared with other processes reported,[10] this reflects our interest in developing a green and sustainable process employing water as the solvent, which is known to afford poorer HMF yields than organic solvents, such as DMSO (which facilitates sugar dehydration but is not a practical solvent for large-scale

DOI: 10.1021/acscatal.5b00965
ACS Catal. 2015, 5, 4345−4352

application). This rationale for selecting an aqueous solvent is simple; all current biomass pretreatment routes to sugars, for example, steam explosion or enzymatic/chemical (acid or base) cellulose hydrolysis, produce aqueous sugar streams;[12] hence, the development of heterogeneous catalysts able to operate in water is essential. It is also important to note that our reaction temperature of 100 °C is significantly lower than most literature reports (>140 °C) to minimize unwanted side reactions and humin formation, which is problematic at high temperature and often poorly quantified. The finding that zirconia monolayers confer excellent hydrothermal stability to SBA-15 suggests that ZrO_2/SBA-15 is a promising support material for more widespread application to aqueous phase reforming.

■ ASSOCIATED CONTENT

Supporting Information

The Supporting Information is available free of charge on the ACS Publications website at DOI: 10.1021/acscatal.5b00965.

Low- and wide-angle XRD patterns, tables with structural parameters and bulk and surface compositions, N_2 porosimetry isotherms and pore size distribution figures, XP spectra, DRIFT spectra for pyridine titration, SO_2 and NH_3 titration and calorimetry figures, tables of catalytic tests for glucose and fructose dehydration to 5-HMF corresponding reaction profiles, normalized activities and recyclability tests, N_2 porosimetry isotherms, and a table of physical properties before and after hydrothermal stability test (PDF)

■ AUTHOR INFORMATION

Corresponding Author

*E-mail: k.wilson@aston.ac.uk.

Notes

The authors declare no competing financial interest.

■ ACKNOWLEDGMENTS

Financial support from the European Union Seventh Framework Programme (FP7/2007-2013) under Grant Agreement No. 604307 is gratefully acknowledged. In addition, we are also grateful to the EPSRC for funding under EP/K014676/1 and for the provision of Leadership Fellowship to A.F.L. (EP/G007594/4). K.W. is grateful to the Royal Society for the award of an Industry Fellowship (IF100206). J.A.M. and G.M. gratefully acknowledge the "Ministerio de Ciencia e Innovación" of Spain through the project CTQ2011-28216, and the Regional Government of Madrid through the project S2013-MAE-2882. Dr. Mark Isaacs is also acknowledged for his assistance with XPS measurements.

■ REFERENCES

(1) Jakob, M.; Hilaire, J. *Nature* **2015**, *517*, 150−152.
(2) Huber, G. W.; Iborra, S.; Corma, A. *Chem. Rev.* **2006**, *106*, 4044−4098.
(3) Kamm, B. *Angew. Chem., Int. Ed.* **2007**, *46*, 5056−5058.
(4) Coombs, J.; Hall, K. *Renewable Energy* **1998**, *15*, 54−59.
(5) Fatih Demirbas, M. *Appl. Energy* **2009**, *86* (Supplement1), S151−S161.
(6) Tuck, C. O.; Pérez, E.; Horváth, I. T.; Sheldon, R. A.; Poliakoff, M. *Science* **2012**, *337*, 695−699.
(7) Dashtban, M.; Gilbert, A.; Fatehi, P. *RSC Adv.* **2014**, *4*, 2037−2050.
(8) Bozell, J. J.; Petersen, G. R. *Green Chem.* **2010**, *12*, 539−554.
(9) Agirrezabal-Telleria, I.; Gandarias, I.; Arias, P. L. *Catal. Today* **2014**, *234*, 42−58.
(10) van Putten, R.-J.; van der Waal, J. C.; de Jong, E.; Rasrendra, C. B.; Heeres, H. J.; de Vries, J. G. *Chem. Rev.* **2013**, *113*, 1499−1597.
(11) Peterson, A. A.; Vogel, F.; Lachance, R. P.; Froling, M.; Antal, J. M., Jr.; Tester, J. W. *Energy Environ. Sci.* **2008**, *1*, 32−65.
(12) Giang, C.; Osatiashtiani, A.; dos Santos, V.; Lee, A.; Wilson, D.; Waldron, K.; Wilson, K. *Catalysts* **2014**, *4*, 414−426.
(13) Stöcker, M. *Angew. Chem., Int. Ed.* **2008**, *47*, 9200−9211.
(14) Elmekawy, A. A.; Shiju, N. R.; Rothenberg, G.; Brown, D. R. *Ind. Eng. Chem. Res.* **2014**, *53*, 18722−18728.
(15) Serrano-Ruiz, J. C.; Luque, R.; Sepulveda-Escribano, A. *Chem. Soc. Rev.* **2011**, *40*, 5266−5281.
(16) Osatiashtiani, A.; Lee, A. F.; Brown, D. R.; Melero, J. A.; Morales, G.; Wilson, K. *Catal. Sci. Technol.* **2014**, *4*, 333−342.
(17) Grecea, M. L.; Dimian, A. C.; Tanase, S.; Subbiah, V.; Rothenberg, G. *Catal. Sci. Technol.* **2012**, *2*, 1500−1506.
(18) Fang, H.; Wan, T.; Shi, W.; Zhang, M. *J. Non-Cryst. Solids* **2007**, *353*, 1657−1661.
(19) Wong, M. S.; Huang, H. C.; Ying, J. Y. *Chem. Mater.* **2002**, *14*, 1961−1973.
(20) Wu, Z.-G.; Zhao, Y.-X.; Liu, D.-S. *Microporous Mesoporous Mater.* **2004**, *68*, 127−132.
(21) Flego, C.; Carluccio, L.; Rizzo, C.; Perego, C. *Catal. Commun.* **2001**, *2*, 43−48.
(22) Infantes-Molina, A.; Mérida-Robles, J.; Maireles-Torres, P.; Finocchio, E.; Busca, G.; Rodríguez-Castellón, E.; Fierro, J. L. G.; Jiménez-López, A. *Microporous Mesoporous Mater.* **2004**, *75*, 23−32.
(23) Bosman, H. J. M.; Kruissink, E. C.; Vanderspoel, J.; Vandenbrink, F. *J. Catal.* **1994**, *148*, 660−672.
(24) Das, S. K.; Bhunia, M. K.; Sinha, A. K.; Bhaumik, A. *J. Phys. Chem. C* **2009**, *113*, 8918−8923.
(25) Krishnan, C. K.; Hayashi, T.; Ogura, M. *Adv. Mater.* **2008**, *20*, 2131−2136.
(26) Ecormier, M. A.; Lee, A. F.; Wilson, K. *Microporous Mesoporous Mater.* **2005**, *80*, 301−310.
(27) Zhu, Y.; Jaenicke, S.; Chuah, G. K. *J. Catal.* **2003**, *218*, 396−404.
(28) Katryniok, B.; Paul, S.; Capron, M.; Royer, S.; Lancelot, C.; Jalowiecki-Duhamel, L.; Belliere-Baca, V.; Rey, P.; Dumeignil, F. *J. Mater. Chem.* **2011**, *21*, 8159−8168.
(29) Gutiérrez, O. Y.; Fuentes, G. A.; Salcedo, C.; Klimova, T. *Catal. Today* **2006**, *116*, 485−497.
(30) Zhang, J.; Ma, Z.; Jiao, J.; Yin, H.; Yan, W.; Hagaman, E. W.; Yu, J.; Dai, S. *Microporous Mesoporous Mater.* **2010**, *129*, 200−209.
(31) Thitsartarn, W.; Kawi, S. *Ind. Eng. Chem. Res.* **2011**, *50*, 7857−7865.
(32) Reyes-Carmona, Á.; Moreno-Tost, R.; Mérida-Robles, J.; Santamaría-González, J.; Maireles-Torres, P.; Jiménez-López, A.; Moretti, E.; Lenarda, M.; Rodríguez-Castellón, E. *Adsorption* **2011**, *17*, 527−538.
(33) Lanzafame, P.; Temi, D. M.; Perathoner, S.; Spadaro, A. N.; Centi, G. *Catal. Today* **2012**, *179*, 178−184.
(34) Chang, B.; Fu, J.; Tian, Y.; Dong, X. *Appl. Catal., A* **2012**, *437−438*, 149−154.
(35) Morales, G.; Osatiashtiani, A.; Hernandez, B.; Iglesias, J.; Melero, J. A.; Paniagua, M.; Robert Brown, D.; Granollers, M.; Lee, A. F.; Wilson, K. *Chem. Commun.* **2014**, *50*, 11742−11745.
(36) Zhao, D.; Feng, J.; Huo, Q.; Melosh, N.; Fredrickson, G. H.; Chmelka, B. F.; Stucky, G. D. *Science* **1998**, *279*, 548−552.
(37) Bruce, D. W.; O'Hare, D.; Walton, R. I. *Local Structural Characterisation: Inorganic Materials Series*; John Wiley & Sons: New York, 2013.
(38) Mitchell, D. F.; Clark, K. B.; Bardwell, J. A.; Lennard, W. N.; Massoumi, G. R.; Mitchell, I. V. *Surf. Interface Anal.* **1994**, *21*, 44−50.
(39) Webb, P.; Orr, C. *Analytical Methods in Fine Particle Technology*; Micromeritics Instrument Corporation: Norcross, GA, 1997.
(40) Zhao, D.; Huo, Q.; Feng, J.; Chmelka, B. F.; Stucky, G. D. *J. Am. Chem. Soc.* **1998**, *120*, 6024−6036.

DOI: 10.1021/acscatal.5b00965
ACS Catal. 2015, 5, 4345−4352

(41) Dondur, V.; Rakic, V.; Damjanovic, L.; Auroux, A. *J. Serb. Chem. Soc.* **2005**, *70*, 457−474.
(42) Emeis, C. A. *J. Catal.* **1993**, *141*, 347−354.
(43) Morterra, C.; Cerrato, G.; Signoretto, M. *Catal. Lett.* **1996**, *41*, 101−109.
(44) Yamamoto, T. *X-Ray Spectrom.* **2008**, *37*, 572−584.
(45) Li, P.; Chen, I. W.; Penner-Hahn, J. E. *Phys. Rev. B: Condens. Matter Mater. Phys.* **1993**, *48*, 10063−10073.
(46) Mountjoy, G.; Anderson, R.; Newport, R. J.; Smith, M. E. *J. Phys.: Condens. Matter* **2000**, *12*, 3505−3519.
(47) Ono, Y.; Hattori, H. *Solid Base Catalysis*; Springer-Verlag: Berlin Heidelberg, 2011; Vol. *101*.
(48) Moliner, M.; Román-Leshkov, Y.; Davis, M. E. *Proc. Natl. Acad. Sci. U. S. A.* **2010**, *107*, 6164−6168.
(49) Yang, B. Y.; Montgomery, R. *Carbohydr. Res.* **1996**, *280*, 27−45.
(50) Chen, C.-Y.; Li, H.-X.; Davis, M. E. *Microporous Mater.* **1993**, *2*, 17−26.
(51) Kim, S. S.; Zhang, W.; Pinnavaia, T. J. *Science* **1998**, *282*, 1302−1305.
(52) Ryoo, R.; Kim, J. M. *J. Chem. Soc., Chem. Commun.* **1995**, 711−712.
(53) Liu, Y.; Pinnavaia, T. J. *J. Mater. Chem.* **2002**, *12*, 3179−3190.
(54) Okamoto, G.; Okura, T.; Goto, K. *Geochim. Cosmochim. Acta* **1957**, *12*, 123−132.
(55) Alexander, G. B.; Heston, W. M.; Iler, R. K. *J. Phys. Chem.* **1954**, *58*, 453−455.
(56) Fournier, R. O.; Rowe, J. J. *Am. Mineral.* **1977**, *62*, 1052−1056.
(57) Morey, G. W.; Fournier, R. O.; Rowe, J. J. *Journal of Geophysical Research* **1964**, *69*, 1995−2002.

DOI: 10.1021/acscatal.5b00965
ACS Catal. 2015, 5, 4345−4352